ELSEVIER

Journal of Molecular Catalysis A: Chemical 131 (1998) 71–90

JOURNAL OF MOLECULAR CATALYSIS A: CHEMICAL

Using photons and electrons to drive surface chemical reactions [1]

J.M. White *

Center for Materials Chemistry, Department of Chemistry and Biochemistry, University of Texas, Austin, TX 78712, USA

Received 17 June 1997; accepted 22 August 1997

Abstract

Selected examples of non-thermal activation of adsorbate–substrate systems are reviewed. Photon and electron activation leads to a variety of interesting surface chemical reactions, sometimes quite selective. Comparisons of photon and electron excitation are emphasized in this paper that focuses on work in our laboratory involving small hydrocarbons, sulfur dioxide, trifluoromethyl iodide and methyl nitrite adsorbed on either Pt(111) or Ag(111). © 1998 Elsevier Science B.V.

Keywords: Photons; Electrons; Surface chemical reactions

1. Introduction

Over the last decade, non-thermal activation of chemical reactions at adsorbate–substrate surfaces has become a subject of great interest among surface scientists and engineers. Using photons, electrons and hyperthermal particle beams, researchers have explored the details of molecular level events that lead from adsorbed reactants to products, both adsorbed and ejected. This paper focuses on activation using photons and electrons. Compared to gas phase, adsorbate–substrate systems are richer because of the roles played by the substrate. The examples selected for emphasis in this paper illustrate this added complexity both in the excitation and the subsequent non-thermal chemistry.

While non-thermal surface reaction chemistry has numerous potential technical applications (e.g., harvesting solar energy, photocatalytic degradation of pollutants in water streams, and selective growth of electronic materials and device structures), we continue to have a keen interest in understanding fundamental questions about excitation, energy transfer and lifetime characteristics of excited states, adsorbate–substrate charge transfer, the minimum energy needed for bond dissociation, and the overall process dynamics.

Historically, early studies of adsorbate photoprocesses focused mainly on semiconductor and insulator surfaces. While these substrates continue to be explored, numerous non-thermal photochemical reactions have also been observed on metal surfaces. Photon-driven chemistry at adsorbate substrate interfaces has been examined using continuous and pulsed sources, both coherent (laser) and incoherent (arc and filament) sources. With the advent of reliable

* Corresponding author.

[1] Dedicated to the memory of Brian Bent whose work stimulated much of our own and whose pleasant encouragement never failed.

PII S1381-1169(97)00257-4

femtosecond laser sources, an important body of literature has emerged describing novel adsorbate chemical processes, many of them involving multiple photons [1]. These lie outside the scope of this paper.

For electrons, much of the early work focused on aspects other than chemical reactions. One example is the elegant use of electron-stimulated desorption as a tool to reveal the local structure of adsorbates [2]. More recently, and a topic of discussion here, electrons have been used to synthesize catalytically interesting adsorbed fragments, sometimes very selectively.

The purpose of this paper is twofold—first, to overview some key concepts that guide the interpretation and understanding of non-thermal activation and relaxation events and, second, to present illustrative examples where photon- and electron-stimulated data are available for comparison. Among the examples, we discuss adsorbed hydrocarbons where electron irradiation leads to very selective bond breaking in some, but by no means all, cases. For methane, comparisons of photon- and electron-stimulated processes provide valuable insights. We also discuss alkyl halides, particularly adsorbed CF_3I, which on Ag(111) exhibits a striking array of photon- and electron-driven reactions. Sulfur dioxide is used to illustrate that, for a fixed adsorbate coverage, the method of preparing that coverage can have a major influence on cross-sections for various processes. Methyl nitrite, CH_3ONO, is used to illustrate the value of angular-dependent desorption measurements. Finally, and for reasonable completeness, other examples are listed.

2. Key concepts

Before undertaking the discussion of some specific cases, we present an overview of some key concepts involved in thermal, photon and electron activation of an adsorbate–substrate system. In this overview, the roles played by the degrees of freedom in the separate components are indicated, for example, absorption of a photon by the isolated adsorbate or substrate. In addition, emphasis is given to the coupling between the adsorbate and substrate degrees of freedom before, during and after either photon absorption or the initial electron-scattering event.

2.1. Thermal activation

Chemical reactions activated thermally typically involve only electronic ground-state reactants. This simplifies treatment of the results but at the same time limits the accessible configurations that can lead to products. To meet the activation energy requirements and reach the activated complex configuration, sufficient energy, E_a, must accumulate and be localized in a reaction coordinate. Typically, this coordinate involves a small number of molecular coordinates, often simplified to a single coordinate, e.g., stretching a bond or rotating around a bond axis. The probability of realizing this configuration is governed by Boltzmann statistics, including the factor $\exp\{-E_a/RT\}$, and can be thought of on the individual molecule or coordinate level as activation by means of statistical energy flow among the coordinates. This flow is the result of couplings between modes. For example, within a given molecule, the anharmonicity of vibrational modes couples them and leads to energy flow. Collisions between species also transfer energy between coordinates. Such couplings also control energy flow in adsorbate–substrate systems. Increasing the temperature increases the probability that, at any given instant, the requisite energy will momentarily accumulate in the reaction coordinate. When this occurs, the system can pass through the activated complex region to products. The probability of doing so depends upon the shape of the potential energy surface around the activated complex region and the momentum vector describing the trajectory along which the system enters this region.

In this description, dynamics associated with coordinates other than the reaction coordinate

are not individually or explicitly treated; rather, they are folded into a single statistical factor, a factor typically estimated by assuming thermal equilibrium between the reactants and the activated complex. To compute the pre-exponential factor at this level of approximation requires the vibrational and rotational partition functions of the reactants and the activated complex. With a potential energy surface (theory), these factors are calculable, but experimental data, while often available for the reactants are generally not available for the activated complex.

2.2. Non-thermal activation

Escaping the limitations of averaging associated with thermal activation requires directed and controlled energy input. For more than three decades, this has been emphasized in the gas-phase reaction dynamics community. More recently, it has become an active area in the surface chemistry community with the utilization of hyperthermal molecular beams and photons. Even earlier, the use of electrons to stimulate surface chemistry in adsorbates, particularly stimulated desorption, was being explored and has led to a series of international DIET (desorption induced by electronic transitions) conferences and a valuable series of publications [3,4]. Through 1990, the literature on electron-stimulated desorption has been thoroughly reviewed by Ramsier and Yates [2].

While the focus of this paper is electronic excitation using incident electrons and photons, we briefly comment on the general attributes of hyperthermal molecular beams [5,6]. For surface collisions of hyperthermal molecular beams, the incident momentum and center of mass translational energy are controlled and have magnitudes much higher than the averages characterizing other degrees of freedom. Thus, the relevant potential energy surface(s) are typically the same as for thermal activation; but the distributions of energies and moments in the incident translational coordinates are altered.

2.3. Photon irradiation

Describing photon activation of surface processes, excellent and detailed reviews are available to which the reader is referred. [2] Briefly, photon activation involves at least two potential energy surfaces—the initial ground state and the electronic excited state accompanying photon absorption. As in gas and condensed phase photochemistry and photophysics, additional excited states of the adsorbate often become involved as the system relaxes. And the presence of the substrate often plays a central role by absorbing photons and transferring energy and/or charge to the adsorbate. Furthermore, because the adsorbate and substrate can be strongly coupled electronically, particularly, in the excited states of the system, the optical properties can differ significantly from those of the separated adsorbate and substrate. As an example, for an adsorbate chemically bonded to a metal substrate, descriptions in terms of an organometallic species adsorbed on the metal may be better approximations than descriptions in terms of the metal and a perturbed adsorbate.

Compared to the typical adsorbate, there are orders of magnitude, more degrees of freedom in the typical adsorbate–substrate system. For an electronic excitation initially localized on the adsorbate, the substrate electronic degrees of freedom can quench the excitation and return the adsorbate to its ground electronic state, and this can occur on a time scale that limits chemical events associated with the initial electronic excitation. In the redistribution, total energy is conserved. As one example, suppose the initial electronic excitation is localized on the adsorbate and is followed by adsorbate nuclear motion on the excited state potential energy surface. Further, suppose that quenching occurs by electron-hole pair formation in the substrate. Then a fraction of the initial excitation energy will be retained as vibrational and rotational

[2] For recent reviews, see Refs. [7–12].

excitation of the adsorbate, the remainder appearing, temporarily at least, in the electronic coordinates of the metal. This process would leave a vibrationally excited ground state adsorbate that is not thermally equilibrated with the other degrees of freedom. This can be thought of as 'top down' non-thermal vibrational excitation whereas normal thermal activation would be 'bottom up' and thermally equilibrated.

Experimentally, the distinction is often critical. For coinage metals like silver, thermally activated, 'bottom up', bond dissociation within an adsorbate often requires average energies exceeding those required for molecular desorption. Thus, dissociation does not occur when a cold adsorbate layer is heated. On the other hand, photon irradiation and quenching of the adsorbate–substrate system can direct energy into just a few vibrational coordinates that lead to dissociative surface chemistry because desorption coordinates remain at low temperature.

2.4. Electron irradiation

Against the backdrop of extensive work in the surface physics community dealing with electron-stimulated desorption, controlled electron irradiation is beginning to emerge as a tool for synthesizing surface fragments, among them species proposed in catalytic schemes but never independently and cleanly prepared for study in spectroscopically significant concentrations.

Compared to monoenergetic photons, electrons are much less expensive to generate—a major advantage. On the other hand, especially for organic adsorbates, electrons have often been regarded as causing too much damage to be useful. There are good reasons. First, inelastic scattering cross sections for electrons are much larger than for photons of the same energy. Thus, the effective penetration depth for electrons is much shorter than for photons and, in turn, the energy deposited per unit volume is often much higher. Second, areal incident flux densities (particles cm^{-2} s^{-1}) are typically much higher for electron sources. The combination of both factors often leads to unselective pyrolysis of the adsorbate. However, since the electron flux density can be easily reduced and the electron energy controlled over a very wide range, the effects of photon and electron irradiation can be compared at equivalent areal energy densities (joules cm^{-2} s^{-1}) or, even better, equivalent energy deposition rates per unit volume (joules cm^{-3} s^{-1}).

One way of establishing reasonable areal electron fluences (electrons cm^{-2}) for such comparisons, is to consider that the process occurs with a geometric cross section, i.e., between 10^{-16} and 10^{-15} cm^2. With this cross section, a monolayer would be consumed with a fluence of about 10^{15} electrons cm^{-2}. For a current of 1 μA (6.24×10^{12} electrons s^{-1}) distributed over 1 cm^2, an irradiation of 100 s would be required to consume a monolayer of material. This is tolerable since controlled reproducible exposures for a few seconds are experimentally feasible with typical instrumentation and since the measurement would involve activation of a fraction of a monolayer. On the other hand, in Auger electron spectroscopy, beam currents often exceed 1 μA and irradiated areas are less than 1 mm^2. For this situation the time to consume a monolayer drops below 1 s. Thus, it is easy to understand how conditions typical of electron spectroscopy must be changed to make it possible to limit the activation to submonolayer amounts of adsorbate.

The question of selectivity in electron activation of adsorbates remains open for study. As discussed below, we have examined several systems with electron energies less than 50 eV and find that selectivity varies widely, but can be very high.

The mechanistic aspects of electron activation, relevant to both ejection and retention, are thoroughly described in a recent review [2]. Because of the small mass relative to nuclei, ca. 5×10^{-4}, direct momentum transfer is generally negligible in collisions between electrons and nuclei. For example, a 1 keV electron would transfer less than 1 eV to a H atom, insufficient

to cleave a typical C–H bond (3 to 4 eV). In the work described below, incident electron energies are typically 50 eV or less and, yet, there is clear evidence for bond cleavage, including C–H. Consequently, models involving excitation of electronic degrees of freedom must be involved.

2.5. Temporal evolution

A very general scheme for nonthermal processes, and one which uses concepts familiar to the photochemist, is attributed to Menzel, Gomer and Redhead (MGR) [13,14]. Assuming only one coordinate (x) is important, the idea is modeled using typical diatomic molecule potential energy curves, $V(x)$, in Fig. 1. In this model, the incident electron causes a very general vertical Franck–Condon quantum mechanical electronic transition from the ground state (A) to an excited state of the system (B, C, or D). This occurs for x in the range $a \leq x \leq b$. The nuclear motion that follows on the heels of the electronic excitation depends on the shape and placement of the excited state potential energy surface. In Fig. 1, state B is reached with the lowest energy excitation and is repulsive for all x, state C is energetically nearby but bound and state D, while unbound, is accessible only for much higher energy input. One easily understood example is illustrated; excitation to state B, when the x coordinate is compressed with respect to its equilibrium value, places the system on very repulsive portion of the excited state. This kind of excitation occurs, for example, in the prompt photodissociation alkyl halide (X) molecules. In this case, a nonbonding orbital is partially emptied and an antibonding orbital localized on the C–X coordinate is partially filled. In this excited configuration, the x coordinate stretches, bold portion of Curve B, and accumulates significant momentum on a femtosecond (fs) time scale. This stretching corresponds to just the elongation half of a typical vibrational period, so dissociation would, in the absence of quenching, occur on the time scale of 10^{-13} s (100 fs). Coupling to the substrate electronic degrees of freedom (not explicitly shown) provides a relaxation channel operating on the same time scale that can return the adsorbate to its ground electronic state at, for example, $x = c$. Quenching of dissociation will prevail unless the previously accumulated momentum in coordinate x exceeds that required for dissociation along the ground state potential. As pointed out by MGR [13,14], this simple model contains an interesting prediction for isotopically labeled systems involving light atom ejection: since the time scale for accumulating the required momentum is longer for the heavier of two isotopes, the dissociation yield should drop as the mass increases. This effect has been observed and modeled in numerous cases [15–18].

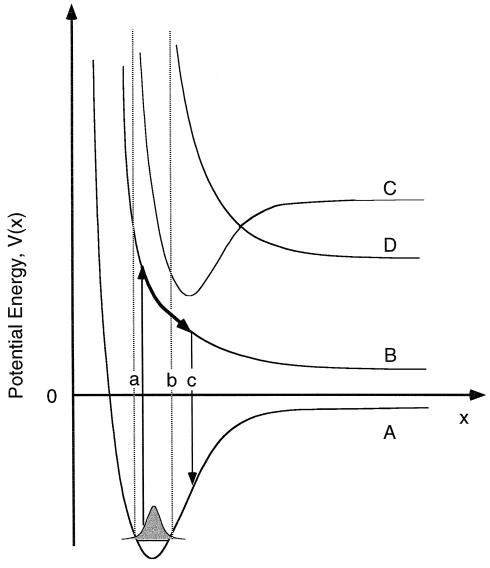

Fig. 1. Single coordinate, x, model description of electronic excitation and relaxation. Franck–Condon excitation to state B occurs within the vibrational envelope (between $x = a$ and $x = b$) of the ground state (A). While in state B, the coordinate x changes, in this case the potential is repulsive, so x lengthens gathering momentum. Quenching occurs, in this case at c returning the system to the electronic ground state with significant momentum in x. Curves C and D represent other electronic excitations.

Antoniewicz extended these ideas, particularly for ionic adsorbate states on metal substrates [19]. For example, assume that the exci-

tation involves transforming a neutral adsorbate to an anion, e.g., electron attachment. The negative adsorbate charge will be accompanied by an image charge of opposite sign in the substrate. The attractive force between these two charges causes the adsorbate–substrate separation to shorten until either the attractive Coulombic forces are balanced by the Pauli repulsive forces that operate in the adsorbate–substrate coordinate or until the anion is returned (quenched) to a neutral state. During this time, the internal coordinates of the adsorbate can be undergoing elongation as in the MGR model. The predictions of the Antoniewicz model are similar to those of MGR except that the center of mass of the adsorbate always moves toward the substrate. If sufficient momentum accumulates in the adsorbate–substrate coordinate during the anion lifetime, quenching will place the neutral ground state at a very repulsive point on the potential energy surface and ejection of the adsorbate (undissociated) will follow unless there is strong coupling (efficient energy transfer) to the phonons of the substrate or to the vibrational modes of neighboring adsorbates.

3. Examples

3.1. Alkyl halides

3.1.1. Overview

Alkyl halides, RX, were among the first adsorbate–metal systems for which monolayer photodissociation was shown to be competitive with quenching [20–22]. These experiments launched a broad range of activities in many labs around the world. The optical properties of the alkyl halides, e.g., CH_3Br, play a key role; the lowest lying gas phase absorption involves excitation from a nonbonding orbital on the halogen to an antibonding C–X orbital. In this excited state, the C–X bond breaks on a 10 fs time scale. It is this short time scale chemistry that makes C–X bond breaking compete effectively with the quenching by the metal. Another property of these molecule–metal systems is the potential for avoiding thermally activated bond breaking, e.g., CH_3Br adsorbs and desorbs from Ag(111) with negligible C–Br cleavage. Thus, nonthermal photon and electron-induced effects are readily distinguished.

The nonthermal chemistry, particularly photon-induced, of monoalkyl iodides, bromides and chlorides has been extensively reviewed and will not be repeated here [7–12,23]. The photon- and electron- driven chemistry of multihalogenated C_1 species containing fluorine have received less attention in the surface science community although such species impact the environment negatively while, at the same time, possessing very desirable technological properties, e.g., lubrication [24] and semiconductor etching [25,26]. In polymer chemistry, low-energy electrons or UV-induced photoelectrons are used to initiate crosslinking in fluorocarbon polymer chains [27–29]. Here, we focus on a prototype, namely, CF_3I.

3.1.2. Properties of CF_3I

Like its monohalogenated analogs, isolated CF_3I, photo-dissociates by breaking the C–I bond on a short time scale [7–12]. Electron interactions are even more pronounced. Among gas phase molecules, CF_3I has an enormous electron attachment cross section, $> 10^{-14}$ cm^2 for electrons near zero eV [30,31]. There is a long range attractive charge–dipole force between the electron and the neutral molecule. As the separation shortens, the lowest unoccupied orbital of the system moves to lower energy and readily accommodates the electron, i.e., a positive electron affinity. [3] This state is dissociative, the C–I bond ruptures and CF_3 and I^- are formed. The molecular crystal structure of CF_3I is interesting, it packs in layers in which all the I atoms are oriented in the same direction but from layer-to-layer alternate in an ‘up’ and

[3] The electron affinity of isolated CF_3I is 1.57 ± 0.2 eV [32].

Table 1
CF_3I as an adsorbate

Substrate[a]	Activation	Key observations	Ref.
Ag(111)	Thermal	Some C–I dissociative adsorption at 105 K (10% of first layer). Two parent TPD peaks at 118 and 126 K (later interpreted as two monolayer orientations[F]). Some thermally ejected CF_3. The only TPD products are CF_3 (310 K) and I (830 K). Preadsorbed atomic I inhibits dissociation.	[34,35] [36]
Ag(111)	Electrons	Dosing between 80 and 85 K, multilayer TPD peak at 100 K. Electron irradiation (100 eV) destroys multilayer with cross-section = 1.1×10^{-16} cm^2. For multilayer, C_2F_3I desorbs at 155 K, CF_2I_2 at 180 K, and C_2F_5 at 340 K. Atomic I inhibits C_2F_5 but allows C_2F_3I and CF_2I_2 to form in first layer of CF_3I.	[37]
Ag(111)	Photons	C–I, but no C–F, bond breaking at all coverages. Wavelength dependent I^-, I and CF_3 ejection from multilayers. CF_3 time-of-flight indicates direct and substrate-mediated processes. AT 193 nm, evidence for intermolecular charge transfer.	[38,39]
Pt(111)	Thermal	Nondissociative adsorption at 85 K. Multilayer TPD peak at 100 K. During TPD, significant thermal dissociation of monolayer along two paths. C–I cleavage to form adsorbed CF_3 and I and C–F cleavage to form CF_2 and IF. CF_3 radicals desorb at 625 K and atomic I at 830 K. CF_2 ejected as it forms (150 K).	[40]
Ru(0001)	Thermal	Some C–I dissociation during dosing at 100 K. During TPD, C–I and C–F bond breaking below 200 K. CF_4 desorption at 605 K and CF_3 at 750 K. Atomic I desorption above 900 K, CF_2 at 1165 K and F at 1225 K.	[24]
Ru(0001)	Electrons	ESDIAD study monitoring F^+. A central beam and three different hexagonal F^+ patterns. Attributed to tilted CF_3, to F adsorbed at step and defect sites, to two large C_{3v} orientations and to a smaller pattern of CF_3 generated by electron-induced decomposition.	[41]
Ni(100)	Electrons	Thermal dissociation during dosing or TPD; complete dissociation only at low coverages. Parent desorption at 150 K. NiF_2 peak at 885 K. Atomic I desorbs at $\sim$1100 K. 110 eV electron irradiation destroys parent TPD peak with cross section of 1.5×10^{-16} cm^2. Atomic F dominates ejected fragments and indicates defluorination. Some CF_3 and CF_4 desorption. C–C bonds are formed and lead to TPD of C_2, C_3 and C_4 products at 400 K. C_2F_5 is proposed as key intermediate.	[42]
Ni(111)	Thermal	I desorbs at 975 K, NiF_2 at 820 K, CF_4 at 780 K, parent peaks at 162 and 122 K. Large fraction of monolayer dissociates into atomic C, I and F bound to Ni.	[43]
Ni(100)	Thermal	Approximately 90% of monolayer decomposes. CF_3 desorption at 316 K, parent peaks at 168 and 136 K, I at $\sim$1000 K, NiF_2 at $\sim$800 K.	[44]

[a] Substrates all below 110 K during adsorption.

'down' configuration [33]. The molecular axes are tilted with respect to the crystal axes so that the I atom of one molecule interacts with the CF_3 group it neighbor.

The thermal, electron- and photon-driven chemistry of adsorbed CF_3I have been studied on several substrates—Ag(111), Ni(100), Ni(111), Ru(001) and Pt(111). Table 1 summarizes the experiments and observations.

3.1.3. Thermal chemistry on Ag(111)

Of the metals, Ag(111) exhibits the least capacity for thermal activation and has been the focus of work in our lab. For adsorption between 84 and 90 K, the first layer is saturated at a CF_3I-to-surface silver atom ratio of 0.30, here this is defined as 1 ML. [4] Of this, 0.10 ML dissociates, forming CF_3(a) and I(a), and the remainder is molecularly held. For $\theta < 0.50$ ML, the nondissociatively adsorbed CF_3I is oriented with the C–I bond parallel to the surface, while at higher coverages all the CF_3I reorients with the C_{3v} axis tilted toward the surface normal. Upon heating, there is some additional dissociation. Multilayers desorb at 100 K, two orientations in the first layer desorb at 110 and 128 K. When dissociation occurs the iodine is retained

[4] In the cited references, quoted coverages are sometimes normalized to the surface atom density of Ag(111). Multiply the numbers quoted in those papers by 3.33 to convert to values quoted here.

but some of the CF_3 is ejected, depending on the CF_3I orientation. Retention occurs for low coverages, where the CF_3I adsorbs with the C_{3v} axis parallel to the surface [45].

3.1.4. Photochemistry of CF_3I on Ag(111)

Detectable photochemistry of adsorbed CF_3I occurs at all coverages from submonolayer through multilayers thick enough to remove all interactions with the underlying metal. One of the very interesting properties of the CF_3I–Ag(111) system is the observation of I^- ejection during irradiation, but only in multilayers, Fig. 2. The coverage dependence is strongly dependent on wavelength (248 vs. 193 nm). For both wavelengths, no I^- is detected below monolayer coverage. For higher coverages up to about 3 ML, the yield grows nearly linearly and is $\sim$10-fold larger at 193 nm. Above 3 ML, the yield at 248 nm decays sharply while that at 193 nm continue to rise approaching saturation between 5 and 10 ML.

These results are described using two channels for the formation of I^-. The first, substrate-mediated charge transfer, is important at both wavelengths and occurs only near the interface, ≤ 3 ML. The yield at 248 nm drops above 3 ML because substrate-mediated events

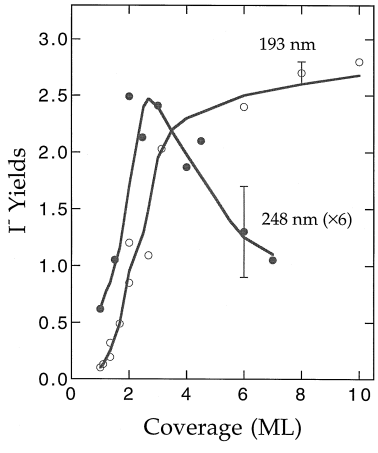

Fig. 2. Ejected I^- yield accompanying 193 nm and 248 nm excimer laser excitation of CF_3I on Ag(111) as a function of CF_3I coverage. The coverage axis is defined in terms of the amount of CF_3I required to cover the Ag surface (from Ref. [38]).

are attenuated by inactive overlayers of CF_3I. The second channel, important only at 193 nm, is independent of the substrate. Charge transfer within a $(CF_3I)_x$ complex is proposed. Schematically,

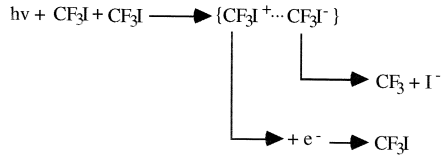

where $\{CF_3I^+ \cdots CF_3I^-\}$ denotes a molecular charge transfer complex. Process 1a will increase with CF_3I coverage until both the short- and long-range effects of the Ag substrate become negligible and until the I^- escape depth is exceeded. Direct evidence for process (1b) is lacking. Photoionization, followed by electron capture, is ruled out on energetic grounds (the ionization potential of CF_3I, 10.23 eV, exceeds the photon energy, 6.4 eV).

The anionic portion of the ion pair $CF_3I^+ \cdots CF_3I^-$ is very dissociative [46–50]. In fact, the dissociation is known to be 'impulsive,' with the majority of the excess energy deposited into the translational energy of the fragments. This enables measurable desorption of I^- even though the polarization force between I^- and its image charge in the metal must be overcome. Unlike substrate mediation, where only one CF_3I molecule is required, process (1) requires clusters. Upon direct excitation of such donor–acceptor clusters, an electron is directly excited from the HOMO of the donor molecule to the LUMO of the acceptor molecule. The plausibility of the idea has been established in recent calculations [51].

In addition to I^-, neutral CF_3 and I are detected by TOF, confirming photodissociation of the C–I bond. The temporal distribution of CF_3 is noteworthy and can be adequately described as the superposition of two channels. The first, a broad, low velocity peak, varies with wavelength and coverage, just like I^-, and is attributed to the CF_3 produced in reaction

(1a) [38]. The second channel, detected as a higher velocity peak, is attributed to direct photodissociation of CF_3I. At 248 nm, where direct absorption involves A band ($5p\pi \rightarrow a_1\ \sigma^*$ transition) excitation, gas phase dissociation produces two electronic states of the atomic I [52–54]:

$$CF_3I + 248\,nm \rightarrow CF_3 + I\left(^2P_{3/2}\right) \quad (2)$$

$$CF_3I + 248\,nm \rightarrow CF_3 + I^*\left(^2P_{1/2}\right) \quad (3)$$

The energy disposal in these two reactions leads to two fast CF_3 peaks, that from Eq. (2) being faster than that from Eq. (3). Confirming the role of direct dissociation of adsorbed CF_3I at 248 nm, we find two peaks in the fast portion of the CF_3 TOF spectra [38], Fig. 3. Similar evidence for direct photodissociation has been reported by Garrett et al. [55] using CH_3I on insulator substrates.

The evidence for adsorbate–substrate coupling makes alteration of the substrate become interesting. For the CF_3I–Ag(111) system, we have followed two strategies: (1) place a photochemically inert spacer layer (hexane) between the metal and the substrate, and (2) cover the Ag(111) with an ordered overlayer of atomic I. The effect of hexane is to inhibit the influence

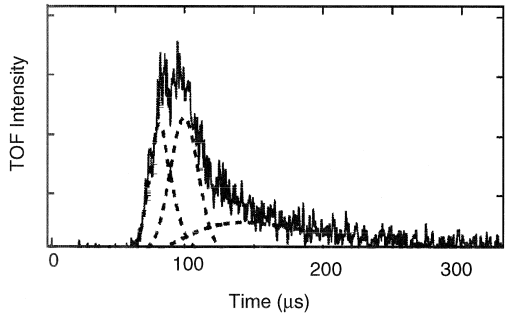

Fig. 3. Time-of-flight distributions measured for CF_3 radicals ejected from a 3 monolayer coverage of CF_3I during 248 nm pulsed laser excitation. The time-of-flight distribution is adequately fit by three modified Boltzmann distributions. The two fastest distributions correspond to direct photolysis forming ground state and electronically excited I (see text) (from Ref. [38]).

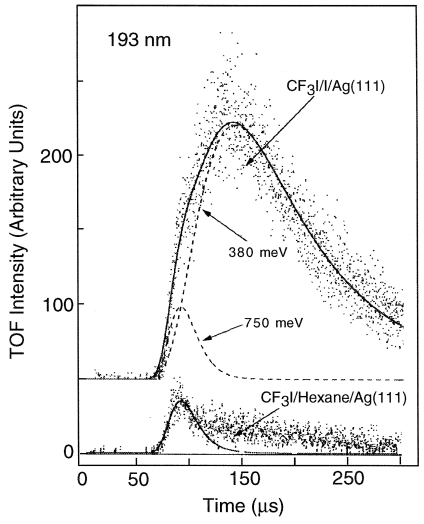

Fig. 4. Time-of-flight distributions for CF_3 radicals ejected during 193 nm irradiation of monolayer CF_3I adsorbed over a monolayer of hexane or atomic I.

of Ag on CF_3I. In these experiments—~25 ML hexane + 2 ML CF_3I,—I^- is ejected at 193 but not 248 nm confirming a role for direct absorption at 193 nm and the dominance of substrate-mediated I^- production at 248 nm [39,56].

The effects of atomic I on the yield of low velocity (charge transfer mechanism) CF_3 are very interesting (Fig. 4)[57]. Controlled I coverages were produced by either thermal- and/or photo-dissociation CH_3I and subsequent removal of residual parent and CH_3 at higher temperatures (~450 K) [58,59]. For iodine coverages below first-layer saturation, the photoinduced charge transfer dissociation follows the substrate work function change; the yields decrease as the work function increases. However, for higher I coverages, the opposite occurs; the work function continues to increase but the yield of CF_3 increases. This increase is substantial and reaches as much as 20–30-fold when the total I coverage increases to 10 layers or more. At this coverage, the low-velocity component of the CF_3 TOF distributions (charge transfer) is about eight times larger than the high-velocity component (direct photodissociation).

This enhancement depends on the wavelength; it is observed at 193 and 248 nm, but not at 308 nm [57].

For a surface reaction mediated by hot substrate carriers, increasing the work often reduces the yield [60]. This observation is generally attributed to the smaller number of hot carriers that have sufficient energy to reach and attach to the adsorbate. While this will account for the lower yield found here at low coverages of I, other means must be found to account for the rising yield at higher I coverages.

We propose that the enhancement is related to the increased charge transfer excitation within an adsorbate/surface complex formed between I and CF_3I. With this model, although the work function increases with I, and lowers substrate-mediated charge transfer, excitation of the proposed I/CF_3I complex, which depends on local properties can still occur and account for the enhanced yield.

Iodine is a known charge-transfer agent; its ionization energy is much smaller than the CF_3I. We assume that 193 and 248 nm, but not 308 nm, photons can promote an electron from the HOMO of the complex, localized on atomic I, into the LUMO of the complex, antibonding in the C–I coordinate and largely localized on CF_3I. This transition can lead to C–I bond cleavage. This charge transfer reaction, in which atomic I or molecular I_2 plays the role of the substrate, differs from conventional substrate-mediated charge transfer reactions in that the excitation and charge transfer is a localized, we could say, direct, excitation. For conventional substrate-mediated charge transfer paths, i.e., most metal or semiconductor substrates, delocalized charge transport and relaxation processes intervene between nascent hot carrier excitation and adsorbate excitation.

3.1.5. Electron chemistry of CF_3I on Ag(111)

Contrasting to the photochemistry on Ag(111) where C–I bonds are broken selectively, there is clear evidence for much less selectivity when electrons are used to activate adsorbed CF_3I. Both C–I and C–F bond breaking occurs on Ag(111) [37], Ni(100) [42,44] and Ru(0001) [41]. Jensen and Thiel studied the thermal and electron-induced chemistry of CF_3I on Ni(100) [42,44]. Thermal activation led to C–I and C–F bond breaking at low coverages, but near-saturation CF_3 desorption began in TPD as C–F cleavage became inhibited. Electron-induced chemistry involved C–I and C–F bond scission with a cross-section of the order 10^{-16} cm^2. CF_xI_y species desorbed at 200 and 240 K; there was evidence for radical (CF) and molecular (CF_4) desorption at 250 K and CF_2 desorption at 350 K. For the first time, carbon–carbon bond coupling of adsorbed fluorocarbons was also seen in the form of C_2F_3I, C_2F_5, C_3F_6, C_4F_8 and C_2F_6 desorbing from 340 to 500 K. Fig. 5, based on Jensen and Thiel's work, illustrates. Clearly, this electron-driven chemistry proceeds with a large cross section and is not selective.

For Ag(111) the conclusions are similar [37]. After electron irradiation there is C_2F_5, CF_2I_2 and C_2F_3I desorption. Reflection absorption infrared spectroscopy (RAIRS) suggests that adsorbed CF_2I_2 has C_{2v} symmetry with both I atoms bound to Ag. C–C coupling to form C_2F_5 is attributed to insertion of CF_2^+ or CF_2, formed

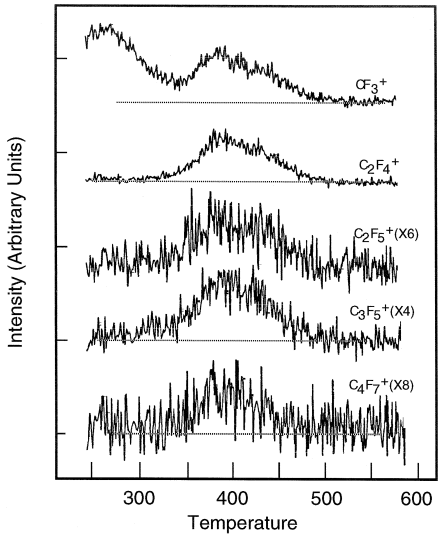

Fig. 5. Desorption of C_n species after electron irradiation of CF_3I on Ni(100). Modified version of Fig. 12 from Ref. [42].

by impact ionization of parent, into previously formed CF_3. At 2.5 ML, the cross section for loss of CF_3I by all removal processes is $1.1 \pm 0.2 \times 10^{-16}$ cm^2, while that for CF_2I_2 formation is $\sim 10^{-17}$ cm^2.

The post-irradiation TPD spectra for electrons and photons have several qualitative similarities. Loss of parent CF_3I molecules is observed as well as reduction of the thermally formed 300 K CF_3 radical peak. A new lower temperature CF_3 radical peak, attributed to CF_3 desorption from sites destabilized by I(a), is seen for both types of excitation. For photon irradiation, however, only C–I bond cleavage is observed, while 100 eV electrons cleave both C–I and C–F bonds, as evidenced by CF_2I_2 formation. C–F bond breaking in the photochemistry experiments is not expected; direct absorption of 248 and 193 nm photons is a $5p\Pi^* \rightarrow \sigma^*$ transition that induces dissociation of the C–I bond. The photoelectrons that are produced, ≤ 2.4 eV, do not have sufficient energy to access the 3.8 eV C–F bond breaking resonance. Another important difference is C–C coupling; neither C_2F_5 nor C_2F_3I is observed following photon irradiation. C–F bond breaking is required to form both of these products and does not occur upon photolysis or subsequent relaxation.

3.2. Sulfur dioxide

Among the systems we have studied, SO_2–Ag(111) exhibits the most interesting dependence of parent photodesorption on preparation method. We focus on that topic here and simply summarize some of the other fascinating details of the photodissociation and photon-driven bimolecular reactions.

As for many adsorbates, there is negligible thermal dissociation when SO_2 is adsorbed at 100 K and subsequently desorbed [61,62]. TPD spectra exhibit evidence for local structural alterations as adsorbates accumulate, i.e., previously adsorbed SO_2 tends to change its structure as more SO_2 is added. What has been termed a 'compressed layer' desorbs at 155 K after saturation of a peak at 176 K (defined as monolayer). Thick multilayers desorb with a peak near 130 K that moves, typical of zero-order kinetics, to slightly higher temperature as the layer thickness increases [62,63].

To summarize, the surface photochemistry, like the gas phase counterpart, is very complex and exhibits wavelength and coverage-dependent properties. In the gas phase, SO_2 exhibits wavelength-dependent UV photochemistry (unimolecular and bimolecular excited state reactions) and photophysics (photon emission) [64–71]. There are no one-photon electronic transitions in SO_2 for energies less than 3.2 eV. These various processes occur with different characteristic lifetimes and probabilities; for example, photodissociation along a very repulsive surface is intrinsically faster than a bimolecular reaction between ground state SO_2 and a triplet excited state of SO_2. The latter is often formed by excitation to a singlet state and conversion to a triplet state. For adsorbed SO_2, these time scale variations are reflected in the coverage dependence. As outlined in the literature, thicker layers of SO_2 or inert spacer are required to observe events that require longer-lived electronically excited SO_2. Roughly, there is no chemistry, other than parent desorption in monolayers, unimolecular processes begin to emerge for two or three layers and a bimolecular reaction leading to SO_3 is only observed after five layers are present.

Likewise, for coverages up to one monolayer, the only electron stimulated desorption (ESD) process is parent desorption, which has a cross-section of $3.6 \pm 0.8 \times 10^{-17}$ cm^2 using 54 ± 1 eV electrons [72] This ESD process has an electron energy threshold of 18.0 ± 1.0 eV corresponding to ionization of the $6a_1$ molecular orbital of adsorbed SO_2 [73–76]. This threshold is high enough to rule out any important contributions from known low-energy electron attachments in isolated SO_2 [77,78]. For coverages greater than one monolayer, ESD is accompanied by electron-induced decomposition (EID)

and the total cross-section for loss of SO_2 is $\approx 10^{-16}$ cm^2, independent of coverage up to 8 ML. The difference between chemisorbed and physisorbed layers is attributed mainly to metal-induced quenching of electronically excited adsorbates, which is less important for those SO_2 molecules further from the metal.

3.2.1. Local orientation

We now turn to the influence of the preparation method on the simplest process–parent SO_2 photodesorption. Near the surface, this process, for which there is no direct gas phase analog, makes a major contribution above a threshold photon energy, 2.3 eV [62], which lies 0.9 eV below the gas phase photon absorption cutoff. This is taken as evidence for substrate-mediated charge transfer to form SO_2^-, the desorption of which illustrates operation of the Antoniewicz mechanism; when the electron is recaptured by the substrate, the SO_2 finds itself in a repulsive configuration with respect to the substrate and is ejected. This process, like cocking and triggering a gun, leads to photodesorption. For multilayers thick enough (>3 ML) to remove the influence of the substrate, SO_2 photodesorption is initiated by direct excitation. One operative mechanism is similar to the 'caging' observed in liquids, where the electronic excitation relaxes into the translational modes of nearby solvent [70,71,79,80].

Fig. 6 makes one of the major points; the adsorbate preparation temperature has an enormous impact on the desorption yield of SO_2. These yields were determined from integrated SO_2 time-of-flight (TOF) distributions, two of which are shown in the inset. If 0.97 ML is dosed at 160 K and then cooled to 100 K for photodesorption, the TOF signal is 10 times larger than if the dosing and irradiation are done at 100 K. But the translational energy distributions are characterized by the same temperature, 650 ± 50 K. As shown by the circles and triangles, this distinction does not disappear until the coverage reaches about 2.5 ML. For the lower curve, adsorption and photolysis were done at

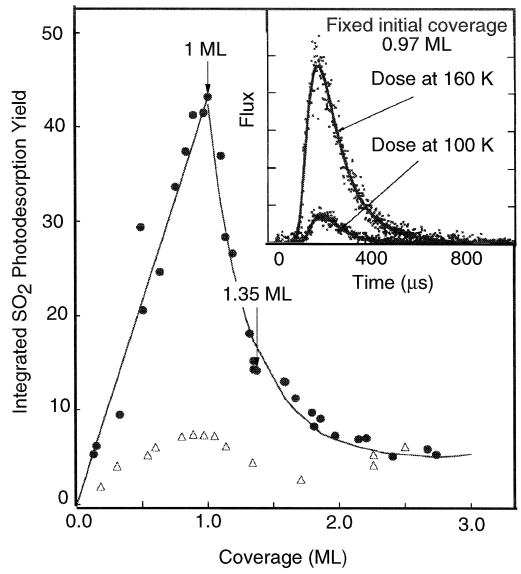

Fig. 6. Integrated time-of-flight signals for photodesorption of SO_2 from Ag(111) as a function of coverage. Monolayer coverage is defined in terms of saturation of a TPD peak attributable to SO_2 bound to Ag. Open triangles correspond to doses and irradiations carried out at 100 K. The upper curve involves annealing the first layer to 160 K (see text). The inset depicts time-of-flight distributions for 0.97 ML of SO_2 prepared by dosing and irradiating at 100 K (low intensity) and by doing at 160 K and irradiation at 100 K (high intensity) (from Ref. [63]).

100 K. For the upper curve, some annealing was involved in the preparation, but the photodesorption was done at 100 K. Submonolayer coverages were dosed at 160 K, monolayer (1 ML) and compressed monolayer (1.35 ML) coverages were prepared by flashing 2.5 ML SO_2 to 160 K and 130 K, respectively. Even higher coverages were produced by dosing SO_2 on top of the annealed monolayer surface. We attribute these yield differences to the detailed structure of the adsorbed SO_2 with respect to the Ag. In separate TPD experiments [63], we showed that dosing at 100 K produces a metastable adsorbed structure. Apparently, this structure is not as readily excited as the equilibrated structure produced at 160 K.

Turning to the upper curve, annealed adsorbates, the formation of a compressed monolayer between 1 and 1.35 ML drastically decreases the photodesorption yield (more than threefold

with an increment of 0.35 ML). This is attributed to a structural rearrangement of the SO_2. TPD and SO_2 adsorption on iodine-covered Ag(111) demonstrate that the compressed monolayer is in intimate contact with the substrate, and that there are strong indications of adsorbate restructuring upon formation of the compressed monolayer [62,63]. As a consequence of this restructuring, the photodesorption yield decreases. That the difference disappears above 2.5 ML is taken as evidence that substrate-independent processes are taking over. Not shown, the coverage dependence above 3 ML continues to rise sharply up to about 7 ML, above which, saturation is slowly approached up to 12 ML, the highest coverage tested. This high coverage behavior is attributed to direct excitation followed by the collisional energy exchange processes described above. Saturation occurs when the escape depth of excited SO_2 is reached.

It is not surprising that substrate-mediated hot electron tunneling into the empty SO_2 orbitals is sensitive to molecular orientation. Assuming Franck–Condon electron transfer from Ag to SO_2 (i.e., during the time required for electron transfer, the nuclei do not move), the transition probability that connects the initial and final states will depend on the instantaneous configuration of the participating atoms and their valence (filled and empty) electron orbitals. Variations with local structure of the Franck–Condon factor can account for order of magnitude variations in the excitation probability and, thus, the desorption probability. It is interesting that the thermodynamically stable monolayer structure is more active than the metastable state. This may not be coincidental, because the thermodynamically most stable state selects the optimal ground-state orbital interactions between the SO_2 and Ag(111). According to UPS and $\Delta\Phi$ measurements [62,63], and theoretical calculations [81], SO_2 in its most stable configuration is adsorbed through S at an atop-Ag site; there is net transfer of electron density from the substrate into the $3b_1$ orbital of SO_2; and the lowest unoccupied orbital, very important for electron attachment, is $6b_2$.

3.3. Adsorbed hydrocarbons

To develop an atomic level description of heterogeneous metal-catalyzed reactions, very labile intermediates are often proposed. It is of interest to isolate and study the proposed intermediates in order to verify their structure and reactivity. As noted in Section 2, nonthermal routes offer one means of doing so. In this section, we focus on hydrocarbon intermediates of catalytic interest.

3.3.1. Methane on Pt(111)

3.3.1.1. Adsorbate and substrate properties. Methane, the simplest saturated hydrocarbon, provides interesting comparisons of photon- and electron-induced surface chemistry. Pt(111) has been used for both. Compared to other metals, platinum possesses intermediate ability to activate chemical bonds. Compared to the coinage metals, it is much more active but, with respect to Fe, Ru and early transition metals, it is less active. Thus, it activates some but not all bonds and reassembles the fragments into products that can be desorbed leaving Pt atoms exposed for another reactant-to-product cycle. This behavior is one key reason for its widespread use in heterogeneous catalysis. Adsorbed CH_4 is weakly and reversibly held on Pt(111); monolayers desorb between 70 and 80 K while multilayers desorb between 40 and 50 K [82]. This weak ground-state attraction to Pt is nonetheless important as we show below. For isolated CH_4, there are no low-energy electron attachment states, and the lowest energy optically accessible excited electronic state lies deep in the vacuum ultraviolet (≤ 145 nm) [83]. Optical excitation into the lowest excited state leads to C–H bond breaking.

3.3.1.2. Surface photochemistry. Based on the above information, it is not surprising that ultra-

violet irradiation of adsorbed layers with wavelengths ≥ 250 nm leads to no evident chemistry (D.J. Alberas-Sloan, J.M. White, unpublished). It is striking, however, that irradiation of monolayer CH_4 with 193 nm photons produces $CH_{3(a)}$ and $H_{(a)}$ and is characterized by a non-negligible cross-section of order 10^{-19} cm^2 [84]. There is good evidence that only CH_4 in direct contact with the metal is involved; there is strong inhibition if a layer of Xe lies between CH_4 and Pt. These results evidence the importance of coupling between the adsorbate and substrate electronic states (see below). One note of contrast: in analogous experiments in which cyclopropane, C_3H_6, adsorbed on Pt(111) was irradiated with 193 nm radiation, the cross-section for loss of parent was less than 10^{-21} cm^2 [85].

First-layer symmetry changes are significant. Isolated CH_4 has T_d symmetry, highly symmetric. In the first layer, this symmetry is lowered to C_{3v}, detectable using reflection absorption infrared spectroscopy (RAIRS) [86]. In C_{3v}, electronic degeneracies are lifted and the energies of some electronic states increase while others decrease. These considerations apply to both occupied and unoccupied states.

In this system, absorption occurs mainly in the metal and energetic electrons are produced. These cannot account for the observed chemistry for the following reasons: (1) in the direct electron irradiation studies (see below), there is no evidence for dissociative chemistry below 10 eV [82]. There is evidence for a resonance at 2.5 eV in solid films of CH_4 [87] and a conduction band located between -0.2 and 2 eV with respect to the vacuum level [88], but there is no evidence for dissociative chemistry associated with these excitations.

Thus, the most likely interpretation of the photochemistry is as follows: CH_4 in direct contact with Pt(111) possesses an electronic structure due to mixing of CH_4 and Pt orbitals that makes direct excitation of the adsorbate–substrate complex energetically accessible. The initial and final electronic states, while still dominated by CH_4 character, contain non-negligible Pt character. CH_4 not in contact with Pt and CH_4 surrounded by fragments is less strongly adsorbed and retains T_d symmetry and is not excited.

3.3.1.3. Surface electron chemistry. Fig. 7 shows how 50 eV electrons changed the character of the subsequent methane TPD spectra. In each case, 1 ML of CH_4 was dosed on a Pt(111) surface at 55 K and then exposed to the fluence of electrons indicated in the figure [82]. The uppermost curve, no electron irradiation, shows a single methane desorption sharply peaked at 78 K. This 78 K desorption feature decays rapidly, nearly vanishing after an exposure of 9.2×10^{15} electrons cm^{-2}. A new peak appears at 250 K and, based on independent work [89,90], is attributed to hydrogenation of surface methyl groups. The small signal around 150 K is a background effect. The cross-section for decay of the 78 K CH_4 peak is of order 10^{-16} cm^2, three orders of magnitude larger than for 6.4 eV photons. As the incident electron energy is lowered, the cross-section drops and has an extrapolated threshold near 8 eV. For compari-

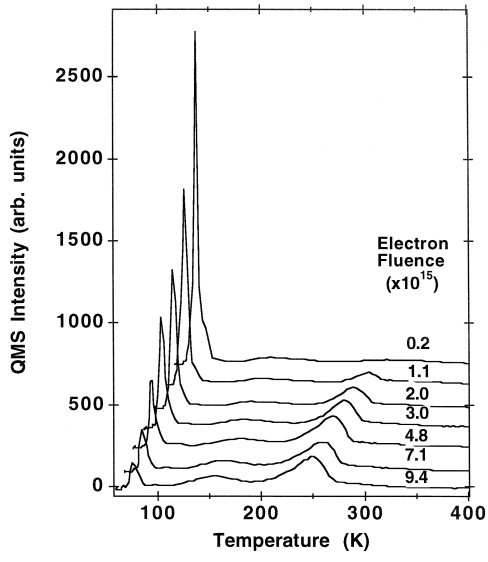

Fig. 7. Effect of electron irradiation on the TPD of monolayer CH_4 adsorbed on Pt(111) (from Ref. [82]).

son, the first ionization potential of CH_4 is 13 eV.

These results have been interpreted as follows. Incident electrons directly excite electrons in orbitals localized on the adsorbed CH_4. This leads to electronic excitations to form both neutral and ionic states of adsorbed CH_4 that dissociate in competition with quenching. From a synthesis perspective, there are two important results. First, so long as the fluence is controlled, the process is very selective, breaking only one C–H bond to form strongly chemisorbed H and CH_3. Second, the primary product, CH_3, is very stable with respect to further electron-induced degradation; the cross-section for removal is less than 10^{-19} cm^2.

3.3.2. Cyclohexane on Pt(111)

In a related work also exhibiting selectivity, cyclohexane adsorbed on Pt(111) and Sn-covered Pt(111) was irradiated with 50 eV electrons [91,92]. The cross-section for loss of monolayers was negligible, $< 10^{-18}$ cm^2. However, multilayers were destroyed with a cross-section of order 10^{-15} cm^2 and the dominant retained product was cyclohexyl bound to the metal. Two possible paths leading from multilayer cyclohexyl to chemisorbed cyclohexyl were suggested—(1) migration of cyclohexyl out of the multilayer displaces cyclohexane at the Pt surface and (2) cyclohexyl abstracts H from cyclohexane located at the Pt surface. To distinguish between the two, cyclohexane was adsorbed over a chemisorbed layer of *n*-butane. Chemisorbed cyclohexyl was formed, and there was no evidence for H-abstraction by cyclohexyl to leave chemisorbed butyl species.

Compared to monolayer methane, monolayer destruction of cyclohexane occurs much less readily. Since the electron excitation cross-section will be at least as large, and likely larger for cyclohexane, we ascribe this difference to the quenching portion of the overall process. It appears that, for monolayers, the quenching of $C_6H_{12}^+$ is much more competitive with C–H bond breaking than in the case of CH_4^+.

3.3.3. Benzene on Ag(111)

3.3.3.1. Photons. Even though benzene absorbs [93], no photoeffects were observed with ultraviolet light from a high-pressure Hg arc lamp (≤ 5.3 eV photon energy). This is attributed to the relatively long times involved in the photodissociation of benzene. Bound excited states are involved, as in curve C of Fig. 1, making it more difficult to compete with substrate quenching.

3.3.3.2. Electrons. The interaction of electrons with C_6H_6 adsorbed on Ag(111) illustrates the feasibility of bond selective chemistry in weakly chemisorbed layers [93,94]. On Ag(111) at 100 K, C_6H_6 adsorbs molecularly, and it desorbs between 208–220 K with no decomposition [93]. After exposure to electrons, only $C_{12}H_{10}$ and H_2 are observed as reaction products in TPD, indicating selective decomposition of C_6H_6 (Fig. 8). By irradiating C_6D_6 with electrons, heating to 300 K to remove parent benzene, and

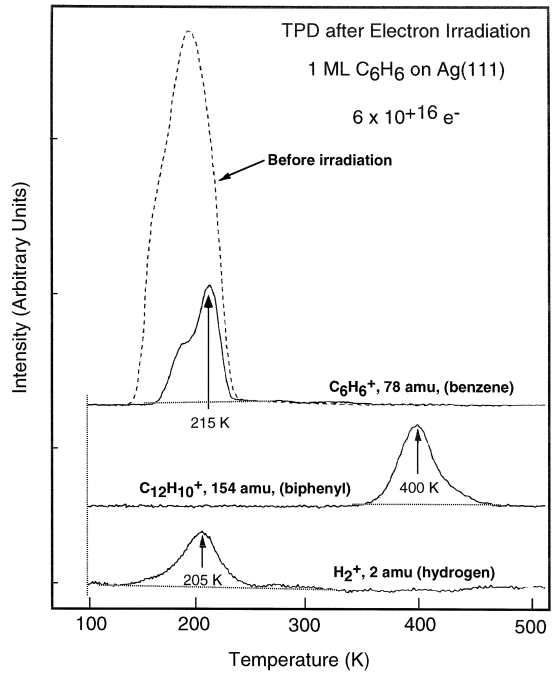

Fig. 8. TPD before (dashed) and after (solid) electron irradiation of 1 ML C_6H_6 molecularly held on Ag(111) at 100 K. The only reaction products are H_2 and $C_{12}H_{10}$ (biphenyl).

after cooling to 100 K, dosing with iodobenzene (C_6H_5I) we demonstrated that biphenyl was not formed during electron irradiation or heating to 300 K; the resulting TPD spectrum (Fig. 5) was dominated by $C_{12}H_5D_5$, not $C_{12}D_{12}$. The decomposition cross-section is of the order 10^{-17} cm^2 between 30 and 50 eV. Since the EID threshold is > 11 eV, an electron impact ionization process, i.e., $C_6H_6(a) \rightarrow C_6H_6^+(a) \rightarrow C_6H_5(a) + H(a)$, was proposed. Electron impact ionization occurs above 9 eV [95,96].

The selectivity indicates that $C_6H_5(a)$ is much less vulnerable to electron-induced decomposition, i.e., compared to the parent ion, $C_6H_6^+(a)$, neutralization of ionized product $C_6H_5^+(a)$, is significantly faster because of stronger coupling to Ag. As a result, C–H and C–C dissociation of $C_6H_5(a)$ occurs with relatively low probability compared to C–H dissociation of $C_6H_6(a)$.

3.3.4. Ethylene on Ag(111)

After electron irradiation of 1 ML of C_2H_4 on Ag(111), the only TPD reaction products are H_2 ($m/e = 2$) at 197 K [97] and C_4H_6 (1,3-butadiene, $m/e = 54$) at 325 K [94]. There is good evidence that vinyl, C_2H_3, is the only hydrocarbon precursor formed, and it leads to C_4H_6 by recombination. The reactions of vinyl with methyl and ethyl fragments, derived from thermal dissociation of CH_3I and C_2H_5I [98], lead to propene and butene, respectively. As for methane, cyclohexane and benzene, the selectivity for breaking one C–H bond is quite high. Other experiments show that the vinyl fragment $C_2H_{3(a)}$, is very stable with respect to electron-induced decomposition. Thus, on Ag(111) it is possible to prepare spectroscopically significant concentrations of adsorbed vinyl species in the absence of other coadsorbates—dose ethylene, irradiate with low-energy electrons, warm ($\sim$ 300 K) to remove residual parent and H, and, finally, cool to 100 K for further experimentation.

3.3.4.1. Ethane on Pt(111). By contrast with the selectivity of these experiments, the formation of C_2H_5 from C_2H_6 adsorbed on Pt(111) is much less selective; there is evidence for both C–C and C–H bond breaking induced by electrons (D.J. Alberas-Sloan, J.M. White, unpublished).

3.4. Methyl nitrite on Ag(111)

The thermal chemistry of methyl nitrite, CH_3ONO, is simple; it adsorbs molecularly at 93 K to form monolayers and multilayers which desorb at 122 and 103 K, respectively [99]. [5] Infrared measurements indicate a coverage-dependent molecular orientation in the first monolayer. Near saturation, the C_s plane of CH_3ONO lies near the surface normal and the internal N–O bond is tilted about 45° with respect to the surface normal [100].

The surface photochemistry induced by ultraviolet radiation is very selective for breaking the internal N–O bond to form adsorbed methoxy, CH_3O, and eject NO [99]. The cross-section is wavelength-dependent and of the order 10^{-18} cm^2 between 193 and 350 nm. Using pulsed excimer laser radiation at 248 nm and angle-resolved detection of NO, there is fast NO which peaks $23 \pm 10°$ away from the surface normal [101]. This is qualitatively consistent with the orientation calculated from the infrared results, and supports a model involving direct CH_3ONO photo excitation followed by the prompt dissociation of CH_3ONO along a very repulsive trajectory. There is a slower NO ejection channel that probably contains species formed by electron attachment.

The surface chemistry induced by 50 eV incident electrons is also dominated by N–O bond cleavage, but with an effective cross-section two order of magnitude higher than for photons, ca. 10^{-16} cm^2 [99]. The electron-driven process is less selective than the photochem-

[5] Ref. [99] gives slightly different monolayer and multilayer peak temperatures. The revised peak temperatures were assigned (see Ref. [100]) using data in which the base substrate temperature was lowered to 93 K. This allowed the multilayer to be more fully developed.

istry, i.e., measurable amounts of C–O and C–H bond breaking occur.

From the perspective of catalytic chemistry, irradiating the CH_3ONO–Ag(111) system with photons provides a clean route to adsorbed methoxy. Adsorbing a monolayer of CH_3ONO, irradiating with photons and annealing to 150 K leaves methoxy species. Future experiments will characterize these species structurally and kinetically.

3.5. Other systems

Space precludes detailed discussion of numerous other metal–adsorbate examples including work that focuses on physical aspects rather than chemical reactions. For example, there is a large body of low-energy electron activation work on many adsorbates in which the focus is on the excitation events, including ion formation [102–107]. But there is also an additional number of adsorbate–substrate systems for which the reaction channels have been explored using both photons and electrons. These include, among others, $Fe(CO)_5$ on Ag(111) [108], NH_3 on Pt(111) [109–111] and Ag(111) [112,113], $CH_3COCOCH_3$ on Ag(111) [114,115], NF_3 on Ag(111) [116], CH_3COCH_3 on Ag(111) [117] and CH_3OH on Ag(111) [118].

4. Summary

Nonthermal excitation of adsorbate–substrate systems with photons or electrons is a rich area of surface chemical science. The chemical richness is demonstrated by the examples used here. As exhibited by the adsorbed hydrocarbons and methyl nitrite, electron irradiation sometimes very selectively breaks a single bond. Weakly adsorbed hydrocarbon monolayers are good candidates, particularly when C–H fragmentation forms strongly chemisorbed fragments. Compared to the weakly held parents, these strongly chemisorbed fragments are much less susceptible to electron-induced dissociation, probably because quenching of excited fragments is much faster. Another displacement synthesis strategy, illustrated by the work on cyclohexane, emerges when the first layer does not readily dissociate because of rapid quenching. Electron irradiation of multilayers may selectively break a C–H bond and the resulting hydrocarbon radical, making use of its high chemical potential, can displace weakly held monolayer parent.

The contrast between photon and electron-driven processes is interesting. Electrons with energies high enough to ionize or dissociate the adsorbate, exhibit cross-sections that are typically two orders of magnitude or more higher than for photons up to 6.4 eV. This underscores several important points. First, the distribution of nascent excited states differ; unlike photons, the incident electrons used here deliver much higher energies and, thus, access many more possible reaction channels. Particularly important among these are impact ionization, as in conventional mass spectrometry, and direct excitation to very highly excited neutral states of the adsorbate. For photons, direct excitation is typically limited to one, or a few, low lying excited electronic states of the adsorbate; for example, an electronic excitation from the highest lying occupied molecular orbital (HOMO) to the lowest unoccupied molecular orbital (LUMO).

Second, incident electrons and photons both couple to the metal substrate and scatter inelastically through electron-hole pair excitations. These adsorbate-independent hot carriers scatter and, with some probability, migrate to the metal–substrate interface where they can attach to the adsorbate and promote nonthermal chemistry, e.g., CF_3I on Ag(111). The scattering is very strong so the distribution of arriving carriers will be dominated by low-energy species with energies just above the Fermi level and falling away exponentially towards the maximum dictated by the energy of the incident photon or electron. Since electron attachments depend on resonances with the adsorbate, the

intensity and the energy distribution of the arriving secondaries will impact the cross-section. In addition, the cross-section will be strongly influenced by overlap of the empty adsorbate orbitals with metal orbitals populated with hot carriers. This overlap will depend on the local position and orientation of the adsorbate with respect to the metal atoms. As a result, and illustrated by the SO_2–Ag(111) system, the method of preparing a fixed adsorbate coverage must be examined. Such secondary, metal-mediated processes, must always be considered for both photon- and electron-driven processes.

Adsorbate orientation, often coverage dependent, is reflected in other aspects of nonthermal chemistry. This is illustrated by the angular distribution of ejected NO that peaks well away from the surface normal when CH_3ONO on Ag(111) undergoes direct excitation.

Multilayers often exhibit unique nonthermal chemistry reflected in events monitored at the adsorbate–vacuum interface. This is illustrated by CF_3I that shows substrate-independent wavelength-dependent photochemistry, ejection of I^-, which requires involvement of multiple adsorbate molecules and cannot be attributed to single molecule excitation.

Of relevance to heterogeneous catalysis, nonthermal methods of activation provide potential selective avenues to catalytically interesting intermediates. From this starting point, detailed spectroscopic and kinetic characterization studies of these intermediates become possible.

Acknowledgements

The author acknowledges with gratitude the contributions to this article from the work of colleagues in our research group at the University of Texas. The financial support of our work by the Department of Energy, the National Science Foundation (CHE9319640), and the Robert A. Welch Foundation is gratefully acknowledged.

References

[1] J.A. Misewich, T.F. Heinz, P. Weigand, A. Kalamarides in: H.-L. Dai, W. Ho (Eds.), Laser Spectroscopy and Photochemistry on Metal Surfaces, Part II, Chap. 19, World Scientific, Singapore, 1995.
[2] R.D. Ramsier, J.T. Yates Jr., Surf. Sci. Rep. 12 (1991) 243.
[3] Desorption Induced by Electronic Transitions, Proc. of Sixth Int. Workshop on Desorption Induced by Electronic Transitions (Diet-6), Krakow, Poland, September 26–29, 1994, Elsevier, Amsterdam, 1994.
[4] A.B. Burns, E.B. Stechel, D.R. Jennison (Eds.), Desorption Induced by Electronic Transitions, Proc. of Fifth Int. Workshop on Desorption Induced by Electronic Transitions (Diet-5), Taos, New Mexico, March 31–April 4, 1992, Springer, New York, 1993 (and references to earlier workshops cited therein).
[5] C.B. Mullins, C.B. Rettner, J. Chem. Phys. 94 (1991) 1626.
[6] K.A. Pacheco, B.A. Ferguson, C. Li, S. John, S. Banerjee, C.B. Mullins, Appl. Phys. Lett. 67 (1995) 2951.
[7] W. Ho, Comments Cond. Mat. Phys. 13 (1988) 293.
[8] H.-L Dai, W. Ho (Eds.), Laser Spectroscopy and Photochemistry on Metal Surfaces, Parts I and II, World Scientific, Singapore, 1995.
[9] P. Avouris, R.E. Walkup, Ann. Rev. Phys. Chem. 40 (1989) 173.
[10] X.-L. Zhou, X.-Y. Zhu, J.M. White, Surf. Sci. Rep. 13 (1991) 73.
[11] J.C. Polanyi, H. Rieley, Dynamics of Gas-Surface Interactions, in: C.T. Rettner, M.N.R. Ashford (Eds.), R. Soc. Chem., London, 1990.
[12] X.-Y. Zhu, Annu. Rev. Phys. Chem. 45 (1994) 113.
[13] D. Menzel, R. Gomer, J. Chem. Phys. 41 (1964) 3311.
[14] P.A. Redhead, Can. J. Phys. 42 (1964) 886.
[15] X.-Y. Zhu, M. Wolf, T. Huett, J.M. White, J. Chem. Phys. 97 (1992) 5868.
[16] X.-Y. Zhu, J.M. White, J. Vac. Sci. Technol. A 11 (4) (1993) 2046.
[17] X.-Y. Zhu, M. Wolf, T. Huett, J.M. White, Desorption Induced by Electronic Transitions DIET V, in: A.R. Burns, E.B. Stechel, D.R. Jennison (Eds.), Proc. Fifth Int. Workshop, Springer, Taos, NM, Apr. 1992, p. 63.
[18] X.-Y. Zhu, J.M. White, Phys. Rev. Lett. 68 (1992) 3359.
[19] P.R. Antoniewicz, Phys. Rev. B 21 (1980) 3811.
[20] E.P. Marsh, F.L. Tabares, M.R. Schneider, J.P. Cowin, J. Vac. Sci. Technol. A 5 (1987) 519.
[21] E.P. Marsh, M.R. Schneider, T.L. Gilton, F.L. Tabares, W. Meier, J.P. Cowin, Phys. Rev. Lett. 60 (1988) 2551.
[22] E. Bourdon, J.P. Cowin, I. Harrison, J.C. Polanyi, J. Segner, C.D. Stanners, P.A. Young, J. Phys. Chem. 88 (1984) 6100.
[23] X.-L. Zhou, J.M. White, in: H.-L. Dai, W. Ho (Eds.), Laser Spectroscopy and Photochemistry on Metal Surfaces, Parts I and II, Chap. 25, World Scientific, Singapore, 1995.
[24] M.B. Jensen, U. Myler, C.J. Jenks, P.A. Thiel, E.D. Pylant, J.M. White, J. Phys. Chem. 99 (1995) 8736.
[25] R.M. Robertson, D.M. Golden, M.J. Rossi, J. Vac. Sci. Technol. B 6 (1988) 1632.
[26] J.-L. Lin, J.T. Yates Jr., J. Vac. Sci. Technol. 13 (1995) 178.

[27] R. Rye, J. Polym. Sci. 31 (1993) 357.
[28] G.H. Vurens, C.S. Gudeman, L.J. Lin, J.S. Foster, Langmuir 8 (1992) 1165.
[29] R. Rye, N.D. Shinn, Langmuir 6 (1990) 142.
[30] S.H. Alajajian, K.-F. Man, A. Chutjian, J. Chem. Phys. 94 (1991) 3629.
[31] M. Heni, E. Illenberger, Chem. Phys. Lett. 131 (1986) 314.
[32] P.S. Drazic, J. Marks, J.I. Brauman, in: M.T. Bowers (Ed.), Gas Phase Ion Chemistry, Vol. 3, Academic Press, Orlando, 1984, p. 167.
[33] S.J. Clarke, J.K. Cockcroft, A.N. Fitch, Z. Kristallogr. 206 (1993) 87.
[34] M.E. Castro, L.A. Pressley, J. Kiss, E.D. Pylant, S.K. Jo, X.-L. Zhou, J.M. White, J. Phys. Chem. 97 (1993) 8476.
[35] A. Szabo, S.E. Converse, S.R. Whaley, J.M. White, Surf. Sci. 364 (1996) 345.
[36] K.H. Junker, Z.-J. Sun, T.B. Scoggins, J.M. White, J. Chem. Phys. 104 (1996) 3788.
[37] J.E. Fieberg, A. Szabo, J.M. White, J. Chem. Soc., Faraday Trans. 92 (1996) 4739.
[38] Z.-J. Sun, A.L. Schwaner, J.M. White, J. Chem. Phys. 103 (1995) 4279.
[39] Z.-J. Sun, A.L. Schwaner, J.M. White, Chem. Phys. Lett. 219 (1994) 118.
[40] Z.-M. Liu, X.-L. Zhou, J. Kiss, J.M. White, Surf. Sci. 286 (1993) 233.
[41] M.B. Jensen, J.S. Dyer, W.-Y. Leung, P.A. Thiel, Langmuir 12 (1995) 3472.
[42] M.B. Jensen, P.A. Thiel, J. Am. Chem. Soc. 117 (1995) 438.
[43] K.B. Myli, V.H. Grassian, J. Phys. Chem. 99 (1995) 5581.
[44] K.B. Myli, V.H. Grassian, J. Phys. Chem. 99 (1995) 1498.
[45] A. Szabo, S.E. Converse, S.R. Whaley, J.M. White, Surf. Sci. 364 (1996) 366.
[46] M. Heni, E. Illenberger, Chem. Phys. Lett. 131 (1986) 314.
[47] C.W. Walter, B.G. Lindsay, K.A. Smith, F.B. Dunning, Chem. Phys. Lett. 154 (1988) 409.
[48] S.Y. Tang, B.P. Mathur, E.W. Rothe, J. Chem. Phys. 64 (1976) 1270.
[49] R.N. Compton, P.W. Reinhardt, J. Chem. Phys. 68 (1978) 4360.
[50] P.W. Harland, H.S. Carman, L.F. Phillips, J. Chem. Phys. 93 (1990) 1089.
[51] J.A. Tossell, Surf. Sci. 373 (1997) L434.
[52] P. Felder, Chem. Phys. 143 (1990) 141.
[53] G.N.A. Van Veen, T. Baller, A.E. De Vries, Chem. Phys. 97 (1985) 179.
[54] M.D. Person, P.W. Kash, L.J.J. Butler, Chem. Phys. 94 (1991) 2557.
[55] S.J. Garrett, V.P. Holbert, P.C. Stair, E. Weitz, J. Chem. Phys. 100 (1994) 4626.
[56] Z.-J. Sun, PhD dissertation, Univ. of Texas at Austin, August 1994.
[57] Z.-J. Sun, J.M. White, to be published.
[58] L.J. Gerenser, R.C. Baetzold, Surf. Sci. 99 (1980) 259.
[59] Z.-J. Sun, R.S. Mackay, J.M. White, Surf. Sci. 296 (1993) 36.
[60] F. Solymosi, J. Kiss, K. Revesz, J. Phys. Chem. 94 (1990) 2224.
[61] D.A. Outka, R.J. Madix, G.B. Fischer, G.L. DiMaggio, Langmuir 2 (1986) 406.
[62] M.E. Castro, J.M. White, J. Chem. Phys. 95 (1991) 6057.
[63] Z.-J. Sun, S. Gravelle, R.S. Mackay, X.-Y. Zhu, J.M. White, J. Chem. Phys. 99 (1993) 10021.
[64] X. Chen, A. Federico, H. Wang, B.R. Weiner, J. Phys. Chem. 95 (1991) 6415.
[65] Y.-L. Huang, R.J. Gordon, J. Chem. Phys. 93 (1990) 868.
[66] M. Kawasaki, H. Sato, Chem. Phys. Lett. 139 (1987) 585.
[67] S. Okuda, R.T. Navaneeth, D.H. Slater, J.G. Calvert, J. Phys. Chem. 73 (1969) 4412.
[68] K. Otsuka, J.G. Calvert, J. Am. Chem. Soc. 93 (1971) 2581.
[69] J.N. Driscoll, P. Warneck, J. Phys. Chem. 72 (1968) 3736.
[70] H.D. Mettee, J. Chem. Phys. 49 (1968) 1784.
[71] L.F. Phillips, J.J. Smith, B. Meyer, J. Mol. Spectrosc. 29 (1969) 230.
[72] L.A. Pressley, J. Kiss, J.M. White, M.E. Castro, J. Phys. Chem. 97 (1993) 902.
[73] D.A. Outka, R.J. Madix, Surf. Sci. 137 (1984) 242.
[74] J. Ahner, A. Effendy, K. Vajen, H.-W. Wassmuth, Vacuum 41 (1990) 98.
[75] M.E. Castro, Dissertation, Univ. of Texas at Austin, l991.
[76] I.H. Hillier, V.R. Saunders, Mol. Phys. 22 (1971) 193.
[77] J.B. Hasted, D. Mathur, in: L.G. Christophorou (Ed.), Electron–Molecule Interactions and Their Applications, Vol. I, Academic Press, New York, l984, p. 451.
[78] O.J. Orient, S.K. Srivastava, J. Chem. Phys. 78 (1983) 2949.
[79] A.L. Harris, J.K. Brown, C.B. Harris, Annu. Rev. Phys. Chem. 39 (1988) 341.
[80] N.F. Scherer, L.D. Ziegler, G.R. Flemming, J. Chem. Phys. 96 (1992) 5544.
[81] J.A. Rodriguez, Surf. Sci. 226 (1990) 101.
[82] D.J. Alberas-Sloan, J.M. White, Surf. Sci. 365 (1996) 212.
[83] L.C. Lee, C.C. Chiang, J. Chem. Phys. 78 (1983) 688.
[84] Y. Matsumoto, Y. Gruzdkov, K. Watanabe, K. Sawabe, J. Chem. Phys. 105 (1996) 4775.
[85] T.B. Scoggins, J.M. White, to be published.
[86] J. Yoshinobu, H. Ogasawara, M. Kawai, Phys. Rev. Lett. 75 (1995) 2176.
[87] T. Huang, W.H. Hamill, J. Phys. Chem. 78 (1974) 2077.
[88] G. Perluzzo, G. Bader, L.G. Caron, L. Sanche, Phys. Rev. Lett. 55 (1985) 545.
[89] M.A. Henderson, G.E. Mitchell, J.M. White, Surf. Sci. Lett. 184 (1987) L325.
[90] S.A. Costello, B. Roop, Z.-M. Liu, J.M. White, J. Phys. Chem. 92 (1988) 1019.
[91] C. Xu, B.E. Koel, Surf. Sci. 292 (1993) L803.
[92] C. Xu, Y.-L. Tsai, B.E. Koel, J. Phys. Chem. 98 (1994) 98.
[93] X.-L. Zhou, M.E. Castro, J.M. White, Surf. Sci. 238 (1990) 215.
[94] X.-L. Zhou, A.L. Schwaner, J.M. White, J. Am. Chem. Soc. 115 (1993) 4309.
[95] L.G. Christophorou, R.N. Compton, Health Phys. 13 (1967) 1277.
[96] K.M. Bansal, W. Fessenden, Chem. Phys. Lett. 15 (1972) 21.
[97] X.-L. Zhou, J.M. White, B.E. Koel, Surf. Sci. 218 (1989) 201.

[98] X.-L. Zhou, J.M. White, Catal. Lett. 2 (1989) 375.
[99] L.A. Pressley, E.D. Pylant, J.M. White, Surf. Sci. 367 (1996) 1.
[100] J.E. Fieberg, J.M. White, J. Vac. Sci. Technol. A 15 (1997) 1674.
[101] J.E. Fieberg, G. Szulczewski, J.M. White, to be published.
[102] P. Ayotte, J. Gamache, L. Sanche, J. Chem. Phys. 106 (1997) 749.
[103] M. Akbulut, T.E. Madey, L. Sanche, J. Chem. Phys. 105 (1996) 6032.
[104] L. Sanche, Scanning Microsc. 9 (1995) 619.
[105] P. Rowntree, L. Parenteau, L. Sanche, J. Chem. Phys. 94 (1991) 8570.
[106] T.E. Madey, Surf. Sci. 299-300 (1994) 824.
[107] P. Rowntree, P.-C. Dugal, D. Hunting, L. Sanche, J. Phys. Chem. 100 (1996) 4546.
[108] M.A. Henderson, R.D. Ramsier, J.T. Yates Jr., J. Vac. Sci. Technol. A 9 (1991) 1563.
[109] Y.-M. Sun, D. Sloan, H. Ihm, J.M. White, J. Vac. Sci. Technol. A 14 (3) (1996) 1516–1521.
[110] A.R. Burns, E.B. Stechel, D.R. Jennison, Y.S. Li, J. Chem. Phys. 101 (1994) 6318.
[111] E.B. Stechel, A.R. Burns, D.R. Jennison, Surf. Sci. 340 (1995) 71.
[112] G.J. Szulczewski, J.M. White, J. Vac. Sci. Technol. A 14 (1996) 1552.
[113] A.L. Schwaner, E.D. Pylant, J.M. White, J. Vac. Sci. Technol. A 14 (1996) 1453.
[114] E.D. Pylant, M.J. Hubbard, J.M. White, J. Phys. Chem. 100 (1996) 15890.
[115] E.D. Pylant, K.H. Junker, G. Szulczewski, M.J. Hubbard, J.M. White, J. Phys. Chem. 101 (1997) 4803.
[116] K.H. Junker, J.M. White, Surface Sci., in press.
[117] S.C. Sparks, A. Szabo, G.J. Szulczewski, K. Junker, J.M. White, J. Phys. Chem., submitted.
[118] A.L. Schwaner, J.M. White, J. Phys. Chem., submitted.